New Aproaches for High-Resolution Optical Microscopy

Denis E. Trancă and George A. Stanciu
Center for Microscopy-Microanalysis and Information Processing, University Politehnica of Bucharest, Splaiul Independentei, Bucharest, Romania

1 RESEARCH PROBLEM

The optical microscopy field has been largely developed in the past decade and many efforts have been made to get improvements in respect to the optical resolution. A special attention has been paid to the detection techniques of the evanescent waves, which are not affected by diffraction, but unfortunately they do not propagate into space. Among these techniques, the apertureless Scanning Near-field Optical Microscopy (a-SNOM) (Patane et al., 2004) have been particularly proved efficient in many ways. Usually it is build as an upgrade to an Atomic Force Microscope (AFM) and it make use of an external laser beam, which is focused on the tip of the AFM probe (Brehm et al., 2005). This configuration allows for simultaneous s-SNOM and AFM imaging. The investigation is done by maintaining the probe in a fixed position, and moving the sample point-by-point in a raster scan manner.

Depending on the type of the interaction between the tip, the focused external laser beam and the surface of the sample, three major a-SNOM techniques exist, which return complementary optical information: a) *scattering - Scanning Near-field Optical Microscopy (s-SNOM)* (Knoll and Keilmann, 2000, Hillenbrand, 2007); b) *Fluorescence Apertureless Scanning Near-field Optical Microscopy (FASNOM)* (Fragola et al., 2003, Huang et al., 2006), and c) *Apertureless Scanning Near-field Optical Microscopy with Second Harmonic Generation* (ASNOM-SHG) (Zayats and Sandoghdar, 2001).

In the first approach (s-SNOM), the illuminated nano-tip of the investigating probe is equivalent to an oscillating electric dipole (Brehm et al., 2005). The electric field component of the incident beam creates this dipole in the tip and determines the dipole to oscillate with the same frequency as the electric field intensity. As a result, the oscillating electric dipole will re-emit light, behaving like an antenna. Because in a typical AFM investigation the tip is located in the proximity of the sample, the oscillating dipole will be highly influenced by the presence of the sample's surface. In this case, the surface is equivalent to a mirror dipole (located in the sample, close to the surface), which will interact with the original dipole. The interaction is reciprocal and the light emitted by the oscillating electric dipole will carry optical information related to the optical characteristics of the sample's surface.

The second approach (FASNOM) exploits the fact that metallic and semiconductor nano-structures have complex influence on fluorescence phenomena (Huang et al., 2006). More precisely, it relies on the fact that placing a metallic structure in the proximity of a fluorophore leads to fluorescence quenching or enhancement and also to a modification of both the radiative and the non-radiative rates of the probe, inducing changes in both the fluorescence lifetime and the in emission intensity. These changes can be exploited to obtain sub-wavelength resolution imaging.

The third approach (SHG-ASNOM) is based on a nonlinear optical effect in which either the tip or the sample is SHG active. In this configuration, the local second harmonic field generated at the sample's surface is probed.

While all these approaches are capable of sub-wavelength optical resolution (on the order of curvature radius of the tip, usually few nanometers), the a-SNOM techniques are widely limited by the difficulties in understanding the collected data. This situation is generated by the fact that the existing mathematical models are either incomplete or extremely complicated (Brehm et al., 2005). In the same time, the experimental acquisition data process is highly affected by background light (representing noise), which appear due to multiple light reflections between the sample's surface and the probe's body; this background light arrives on the detector and has a higher intensity than the light emitted from the near-field of the sample, assessing thus difficulties in the detection process.

E. Trancă D. and A. Stanciu G..
New Aproaches for High-Resolution Optical Microscopy.

2 OUTLINE OF OBJECTIVES

The objectives of the presented work are focused on addressing the major issues faced by a-SNOM techniques. Thus, an advancement regarding the mathematical models associated with the physical phenomena is on the objective list. Analyses of the mathematical models will provide clues for improvements with respect to data interpretation process – that is another major objective. Because of the difficulties associated with a-SNOM techniques, few investigation areas had been explored till now. Thus, an increased attention is given to new research areas where a-SNOM can be used successfully – this being the third major objective of the presented work.

3 STATE OF THE ART

In the frame of near-field optical investigations, two major categories of microscopes are available: (a) aperture-SNOM, and (b) apertureless-SNOM. The first class uses a metal-coated tapered optical fibre as a probe (NOVOTNY et al., 1995). Although SNOM with aperture is more popular and already commercially available, it suffers from a major drawback, as a compromise is necessary between the dimension of the aperture and the power of the incident laser beam. For higher resolution, the aperture needs to be smaller; in the same time, for an efficient transmission, a smaller aperture requires a greater optical power, which may be harmful to the probe's tip. This situation limits the lateral resolution to about 100 nm.

The second class of near-field microscopes is represented by the so-called "apertureless-SNOM". Its functioning principle has been already presented in the introductive part of the paper. As this class of near-field microscopes present several advantages over SNOM with aperture (better resolution; independence on the radiation wavelength), it itself confronts with a series of difficulties. The major drawback is the presence of a background light (noise), which affects the detection process. Several techniques have been developed to date in order to discriminate between the near-field signal and the signal generated by the background light. Higher harmonic demodulation (HHD) (Maghelli et al., 2001) takes advantage over the nonlinear dependence of the intensity of the light emitted from the near-field with the distance between the tip and the sample's surface. Thus, oscillating the probe in a sinusoidal movement above the sample (as in AFM tapping mode) and detecting the signal on a higher harmonic of the oscillation frequency f_o, the signal-to-noise ratio (SNR) will increase. This is due to the rather linear dependency of the background light on the tip-sample distance.

However, HHD is not sufficient for efficient background reduction. Along with it, interferometric detection is also used. During the last decade, three major interferometric methods were used: homodyne (Knoll and Keilmann, 2000), heterodyne (Gomez et al., 2006) and pseudoheterodyne detection (Ocelic et al., 2006). Among these, the last one proved to be particularly efficient and easy to implement. Is consists in a modified Michelson interferometer, in which one arm is used for the illumination of the tip and for collection of the near-field emitted light (together with the background). The other arm is travelled by a reference beam, which is phase-modulated by an oscillating mirror. This reference mirror oscillates with a certain frequency M (much smaller than the oscillating frequency of the probe) and certain amplitude, A. The two beams finally interfere on the detection path, on which a detector is placed. Without the reference beam, the Fourier spectrum of the electric signal generated by the detector will contain signal components situated at the probe's oscillation frequency and at its harmonics. When the reference beam is present, the phase modulation determines the appearance of two side-bands around each initial harmonic component. These side-bands contain components situated at $nf_o \pm mM$. It had been demonstrated that the background light has a minimal influence on these side-bands; thus, detection on a frequencies situated in these side-bands assures for best SNR.

A recently reported alternative to pseudo-heterodyne detection is represented by the combination between synthetic optical holography and s-SNOM (Schnell et al., 2014). In this case, the resulting image is a hologram, which contains both amplitude and phase data of the near-field emitted light.

Regarding the mathematical models, two major models are largely used: Oscillating Point Dipole Model (OPDM) (Knoll and Keilmann, 1999) and Finite Dipole Model (FDM) (Cvitkovic et al., 2007).
To date, a-SNOM has been applied successfully in several areas, including: nano-imaging (Schnell et al., 2010), characterisation of plasmonic structures (Kim and Kim, 2012), near-field spectroscopy (Stiegler et al., 2011), nano-chemical characterisation (Berweger et al., 2013), or SHG and fluorescence on representative samples (Huang et

al., 2006, Zayats and Sandoghdar, 2001). The presented work extends the application areas of a-SNOM in areas like biology, electronics and measurement of electric permittivity in the visible domain (using the OPDM). Detailed studies regarding the influence of functioning parameters upon the image contrast in a pseudo-heterodyne scheme was also done (Tranca et al., 2014).

4 METHODOLOGY

The methodology is divided in three sections, which follow the three major objectives described before. Thus, advances in mathematical modelling are represented by improvements regarding the oscillating dipole model (OPDM), which are obtained by advanced mathematical analysis of signal spectra. Theoretical results are correlated with the experimental data in the purpose of advancing the data interpretation process. A quest for new applications for s-SNOM investigations is worked up by using the results obtained in the previous steps and experimental data on samples containing dielectrics or biological tissues.

4.1 Signal Analysis

The intensity of the near-field scattered light σ is proportional with the amplitude of the incident light phasor E_o and a factor α_{eff} named the effective polarizability (Ocelic et al., 2006):

$$\sigma \sim \alpha_{eff} \cdot E_o \tag{1}$$

According to the oscillating point dipole model, the effective polarizability has the form:

$$\alpha_{eff} = \alpha \cdot \frac{\beta(\varepsilon_s)+1}{1-\frac{\alpha \cdot \beta(\varepsilon_s)}{16\pi \cdot (a+\tilde{z})^3}} \tag{2}$$

In Eq. (2), α stands for the polarizability of the tip, and $\beta(\varepsilon)$ depends on the local sample electric permittivity, ε_s by the relation:

$$\beta(\varepsilon_s) = \frac{\varepsilon_s - 1}{\varepsilon_s + 1} \tag{3}$$

Assuming a sinusoidal oscillation of the probe above the sample, this parameter can be written as:

$$\tilde{z} = d_o + \frac{1}{2} \cdot z_o \cdot \left[1+\sin(2\pi f_o \cdot t)\right] \tag{4}$$

Here, d_o is the min. distance between tip-sample during the probe's oscillation above the sample, z_o is the oscillation amplitude of the probe, f_o is the oscillation frequency of the probe and t is time.

Rewriting Eq. (2), the intensity of the near-field scattered light will have the following form:

$$\sigma(\beta,t) = \alpha(\beta+1) \cdot \frac{16\pi \cdot \left(a + d_o + \frac{1}{2} \cdot z_o \cdot \left[1+\sin(2\pi f_O \cdot t)\right]\right)^3}{16\pi \cdot \left(a + d_o + \frac{1}{2} \cdot z_o \cdot \left[1+\sin(2\pi f_O \cdot t)\right]\right)^3 - \alpha \cdot \beta} \cdot E_o \tag{5}$$

From this point, one can spectrally analyse the function given by Eq. (5), by using the exponential Fourier transformation method. According to Fourier analysis, a function can be written as a sum of its harmonic components. In our case, the harmonic components can be written as:

$$c_n = \alpha(\beta+1) \cdot E_o \cdot \frac{1}{2\pi} \cdot \int_{-\pi}^{\pi} \frac{e^{-j \cdot n \cdot u}}{\left[a+d_o+\frac{1}{2}\sqrt[3]{\frac{16\pi}{\alpha \cdot \beta}}(1+\sin(u))\right]^3 - 1} du \tag{6}$$

Although the integration calculus in Eq. (6) is not a common one and its calculation requires special mathematical algorithms, its complexity decreases if it is calculated for certain values of the n factor. Using numerical methods, the definite integral in Eq. (6) can be easily calculated. Thus, for a certain integral positive n and in the case of well-known experimental conditions (regarding the AFM functioning parameters and the characteristics of the probe), the only variable in Eq. (6) remains β.

However, the value of the spectral component c_n cannot be experimentally determined, and this is due to the background light presence. By using the pseudoheterodyne detection scheme and detecting the signal on the side-bands created around every spectral component of the initial signal, the influence of the background light can be bypassed. The detection on a certain component located at $nf_o \pm mM$ can be accomplished by means of a lock-in amplifier. In this case, a reference beam is used and its mathematical form will be (as a Fourier series):

$$E_R = \sum_m \rho_m \cdot \exp(j \cdot m \cdot 2\pi M \cdot t) \tag{7}$$

The coefficients ρ_m can be written as:

$$\rho_m = J_m\left(\frac{2\pi}{\lambda} A\right) \cdot \rho \cdot \exp\left(j \cdot \psi_R + j \cdot m \frac{\pi}{2}\right) \tag{8}$$

Here, ρ is the amplitude of the amplitude of the reference wave phasor, A is the oscillation amplitude of the reference mirror, λ is the wavelength of the beam, M is the oscillation frequency of the reference mirror, Ψ_R is the mean phase difference between the two interferometric pathways and t is time. In Eq. (8), J_m stands for the Bessel function of order m.

The resulting interference signal U between the

near-field light σ will and the reference beam E_R will have the spectral components $u_{n,m}$:

$$u_{n,m} = 2 \cdot \left(real\{c_n\} \cdot real\{\rho_m\} + imag\{c_n\} \cdot imag\{\rho_m\} \right) \quad (9)$$

The above equation expresses the exact form of a single spectral component of the higher harmonic demodulated, pseudo-heterodyned near-field signal. Together with the Eq. (6) and (8), it can be used to develop a detailed analysis of the near-field signal. The main purpose is to understand the way in which the optical parameters of a sample influence the detected signal. In the same time, it is important to understand the way in which every functioning parameter of the system influences the detected signal and the overall image contrast.

4.2 Data Interpretation

As the background light has a minor influence on the components situated at frequencies $nf_o \pm mM$, with $m \neq 0$, a proportional relation can be assumed between the value of an image pixel $I_{n,m}$ and the amplitude of the harmonic component $u_{n,m}$ on which the detection is employed. This can be expressed as a linear mathematical relation. Based on this proportionality, the spectral component c_n from Eq. (9) can be determined. Introducing c_n in Eq. (6), the value for β is obtained and with Eq. (3), the electric permittivity of the investigated material is then determined. Thus, the data obtained by s-SNOM investigation can be interpreted on the basis of the local electric permittivity of the sample. Figure 1 shows two images of a sample containing *Si* and SiO_2 domains. The images were detected at, respectively, $2f_o+M$ and $2f_o+2M$. Both images are necessary for electric permittivity measurement. The figure also shows how the areas of different materials (*Si* and SiO_2) were selected for local permittivity determination.

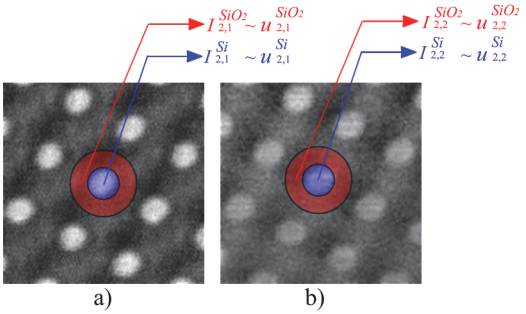

Figure 1: 2x2 µm s-SNOM images of the Si/SiO_2 sample; a) detection on $2f_o+M$; b) detection on $2f_o+2M$. The central Si region is marked with blue and the surrounding SiO_2 region is marked with red.

A crucial role in data interpretation process is played by the functioning parameters of the system, which can easily influence the image intensity and contrast. An example is the oscillation amplitude, A, of the reference mirror. It has been demonstrated that the image contrast is strongly dependent on A and depending on the value of A, the image contrast can be inverted and even reduced to zero. However, the contrast variation is due to variation of the amplitude of the spectral components of the signal with the amplitude A. In Figure 2 is presented the variation of the magnitudes of the spectral components situated at $2f_o+M$ and $2f_o+2M$ with the amplitude A of the reference mirror oscillation.

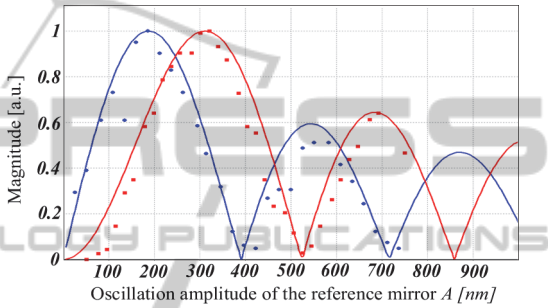

Figure 2: Normalized magnitudes of the spectral components situated at $2f_o+M$ (blue) and at $2f_o+2M$ (red); their variation with the amplitude A of the reference mirror. Continuous curves: Jacobi–Anger expansion coefficients; circled curves: Fast Fourier Transform; Black dots: experimental determinations.

Another example is the mean phase difference Ψ_R between the two interferometric pathways. Varying the mean phase difference, the amplitude of the detected signal will also vary, and every spectral component will be affected. In Figure 3 is presented the variation of the magnitudes of the spectral components situated at $2f_o+M$ and $2f_o+2M$ when the mean phase difference Ψ_R is varied between 0 and 2π.

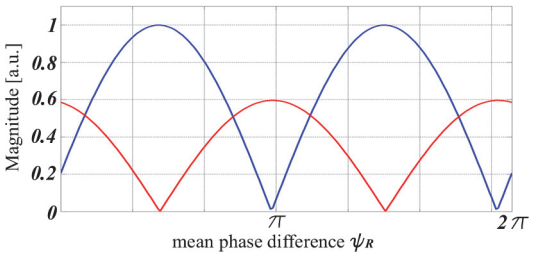

Figure 3: Normalized magnitudes of the spectral components situated at $2f_o+M$ (blue) and at $2f_o+2M$ (red); their variation with the mean phase difference, Ψ_R.

4.3 New Applications

Due to the fact that such a microscopy system can provide local optical information about the investigated sample with sub-wavelength resolution, it became highly attractive for many applications. In biology and medicine, the refractive index of a live cell has gained much attention as an attractive indicator of cell abnormality. In cancer biology, it is well known that the refractive indexes of cancer cells are relatively higher than normal cells, which is believed as a good criterion for quantitative diagnosis of cell malignancy. The possibility to map the electric permittivity of a biologic sample with nano-resolution precision can provide the means for early stage cancer diagnosis.

In materials science, the detailed knowledge of the changes in the refractive index can be used to pinpoint the locations of local defects.

The a-SNOM system can also be used in the nano-electronics industry, where in the last years the optical constants of the materials became important, as they are related to the thickness of the films: errors in the refractive index value translate into errors in the film thickness, determining less accurate results.

4.3.1 S-SNOM Investigations

Two different samples were used for s-SNOM investigations. The first one was a calibration sample containing *Si* and SiO_2 features and it is relevant for nano-electronics industry. It was prepared from a *Si* substrate on which a 26 nm thick SiO_2 film was deposed. Holes with 500 nm in diameter have been made in the SiO_2 film until they reached the *Si* substrate. s-SNOM image containing a single hole, together with the AFM image is presented in Figure 4. The two images were taken simultaneous.

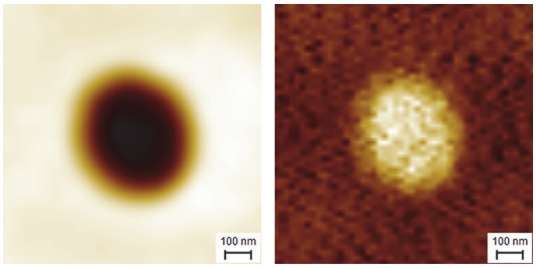

a) b)

Figure 4: a) AFM and b) s-SNOM investigation on a Si/SiO_2 sample.

The second sample for s-SNOM investigations was a biological tissue from a rat retina. In Figure 5 there can be observed retinal ganglion cells. Again, simultaneous acquired AFM and s-SNOM are presented.

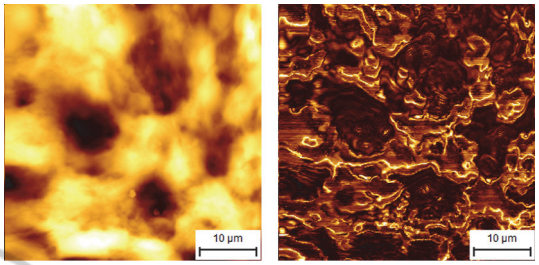

a) b)

Figure 5: a) AFM and b) s-SNOM investigation on a rat retina tissue.

The results presented here demonstrate not only the capability of the s-SNOM system to image samples relevant for micro- and nano-electronics industry and for biology, but they also demonstrate the nanometric-scale optical resolution capability.

4.3.2 FASNOM Investigations

A sample containing collagen fibres deposed on a Si substrate was used to investigate the optical near-field with the modulation of the fluorescence (FASNOM). This sample is also relevant to biology and medicine areas, as the collagen is an important compound of many biological tissues. In Figure 6 are presented the AFM and FASNOM images.

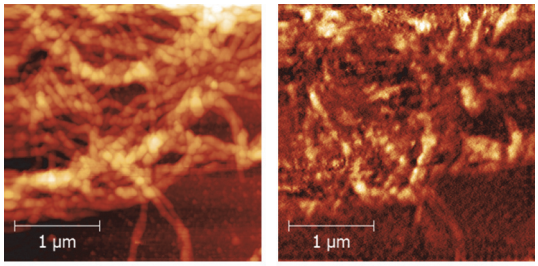

a) b)

Figure 6: a) AFM and b) FASNOM investigation on a sample containing collagen fibres.

4.3.3 SHG-SNOM Investigations

The collagen sample used for FASNOM imaging is also relevant for SHG-SNOM investigation. In Figure 7 are presented the AFM and SHG-SNOM images on this sample.

A second sample on which SHG-SNOM imaging was performed is a rabbit cornea tissue. A good SHG signal was detected, as investigated tissue is

rich in collagen, which is known to generate second harmonic optical frequency light.

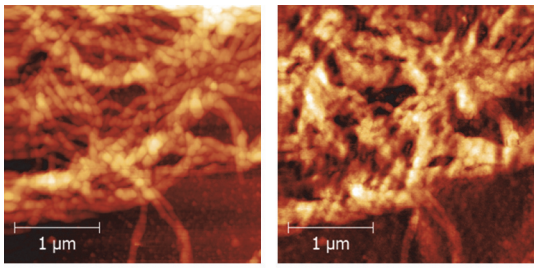

Figure 7: a) AFM and b) SHG-SNOM investigation on a sample containing collagen fibres.

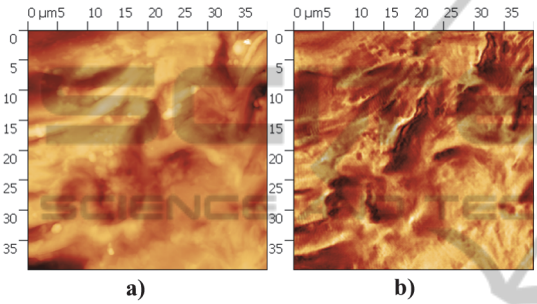

Figure 8: a) AFM and b) SHG-SNOM investigation on a sample containing a rabbit cornea tissue.

5 EXPECTED OUTCOME

Regarding the s-SNOM imaging, the expected outcome is related to the possibility to map at nanoscale precision the local electric permittivity of complex samples, such as biological samples. Such a map can provide useful information regarding the cell abnormality or details of the sub-cellular features. Such investigations are of high importance, as the s-SNOM system does not require special preparations or treatments of the samples. To achieve this, firstly the influence on the detected signal of all involved functioning parameters of the system need to be evaluated. Secondly, investigations in well-known functioning conditions need to be performed on simple samples containing known materials, in order to calibrate the system and to confirm the method for electric permittivity determination. The third major step comes with the complex samples containing biological cells, on which the mapping of the local electric permittivity is performed.

For FASNOM and SHG-SNOM systems, the expected outcome is related to the correlation with their corresponding far-field optical investigations. If their only gain (against the fluorescence microscopy and SHG microscopy, respectively) is the improved resolution, then this is sufficient for new important scientific findings, as fluorescence optical investigations or SHG investigations with nanometric resolution were impossible before. For this, large areas on relevant samples can be investigated both with far-field and near-field methods, in order to find correspondences at micro-scale. If correspondences are possible, then fluorescence and SHG near-field investigations can be performed at nano-scale, which will provide detailed optical data.

6 STAGE OF THE RESEARCH

The stage of the presented research is sufficiently advanced for s-SNOM imaging system. As shown in the Methodology section, the possibility to measure the local electric permittivity with nano-resolution was demonstrated on a calibration sample. New applications for s-SNOM in the biology area are expected, as biological tissues has already been investigated by s-SNOM (see section 4.3.1). The next step is the mapping of the electric permittivity of complex samples containing biological cells. Regarding the FASNOM and SHG-SNOM, the detection capabilities was demonstrated on relevant samples; however, far-field investigations need to be performed on the same samples, in the next steps, in order to compare them with the near-field images.

ACKNOWLEDGEMENTS

This work is supported by the Sectoral Operational Programme Human Resources Development (SOP HRD), financed from the European Social Fund and the Romanian Government under the contract number POSDRU/159/1.5/S/137390/.

REFERENCES

Berweger, S., Nguyen, D. M., Muller, E. A., Bechtel, H. A., Perkins, T. T. & Raschke, M. B. 2013. Nano-Chemical Infrared Imaging of Membrane Proteins in Lipid Bilayers. *Journal of the American Chemical Society,* 135**,** 18292-18295.

Brehm, M., Frey, H., Guckenberger, R., Hillenbrand, R., Kazantsev, D., Keilmann, F., Ocelic, N. & Taubner, T. 2005. Consolidating apertureless SNOM. *Journal of*

the Korean Physical Society, 47**,** S80-S85.

Cvitkovic, A., Ocelic, N. & Hillenbrand, R. 2007. Analytical model for quantitative prediction of material contrasts in scattering-type near-field optical microscopy. *Optics Express,* 15**,** 8550-8565.

Fragola, A., Aigouy, L. & Boccara, A. 2003. Fluorescence apertureless scanning near-field microscopy for high resolution biological imaging. *Novel Optical Instrumentation For Biomedical Applications,* 5143**,** 139-144.

Gomez, L., Bachelot, R., Bouhelier, A., Wiederrecht, G., Chang, S., Gray, S., Hua, F., Jeon, S., Rogers, J., Castro, M., Blaize, S., Stefanon, I., Lerondel, G. & Royer, P. 2006. Apertureless scanning near-field optical microscopy: a comparison between homodyne and heterodyne approaches. *Journal of the Optical Society of America B-Optical Physics,* 23**,** 823-833.

Hillenbrand, R. 2007. Scattering-type near-field microscopy: From nanoscale infrared material recognition to superlens studies. *2007 Pacific Rim Conference on Lasers and Electro-Optics, Vols 1-4***,** 39-40.

Huang, F., Festy, F., Richards, D., Andrews, D., Nunzi, J. & Ostendorf, A. 2006. Fluorescence enhancement and energy transfer near a metal tip. *Nanophotonics-USA,* 6195.

Kim, D. S. & Kim, Z. H. 2012. Role of in-plane polarizability of the tip in scattering near-field microscopy of a plasmonic nanoparticle. *Optics Express,* 20**,** 8689-8699.

Knoll, B. & Keilmann, F. 1999. Near-field probing of vibrational absorption for chemical microscopy. *Nature,* 399**,** 134-137.

Knoll, B. & Keilmann, F. 2000. Enhanced dielectric contrast in scattering-type scanning near-field optical microscopy. *Optics Communications,* 182**,** 321-328.

Maghelli, N., Labardi, M., Patane, S., Irrera, F. & Allegrini, M. 2001. Optical near-field harmonic demodulation in apertureless microscopy. *J Microsc,* 202**,** 84-93.

Novotny, l., pohl, d. & regli, p. 1995. Near-field, Far-field and Imaging Properties of the 2D Aperture SNOM. *Ultramicroscopy,* 57**,** 180-188.

Ocelic, N., Huber, A. & Hillenbrand, R. 2006. Pseudoheterodyne detection for background-free near-field spectroscopy. *Applied Physics Letters,* 89.

Patane, S., Gucciardi, P. G., Labardi, M. & Allegrini, M. 2004. Apertureless near-field optical microscopy. *Rivista Del Nuovo Cimento,* 27**,** 1-46.

Schnell, M., Carney, P. & Hillenbrand, R. 2014. Synthetic optical holography for rapid nanoimaging. *Nature Communications,* 5.

Schnell, M., Garcia-Etxarri, A., Alkorta, J., Aizpurua, J. & Hillenbrand, R. 2010. Phase-Resolved Mapping of the Near-Field Vector and Polarization State in Nanoscale Antenna Gaps. *Nano Letters,* 10**,** 3524-3528.

Stiegler, J. M., Abate, Y., Cvitkovic, A., Romanyuk, Y. E., Huber, A. J., Leone, S. R. & Hillenbrand, R. 2011. Nanoscale Infrared Absorption Spectroscopy of Individual Nanoparticles Enabled by Scattering-Type Near-Field Microscopy. *Acs Nano,* 5**,** 6494-6499.

Tranca, D. E., Stoichita, C., Hristu, R., Stanciu, S. G. & Stanciu, G. A. 2014. A study on the image contrast of pseudo-heterodyned scattering scanning near-field optical microscopy. *Optics Express,* 22**,** 1687-1696.

Zayats, A. V. & Sandoghdar, V. 2001. Apertureless near-field optical microscopy via local second-harmonic generation. *Journal of Microscopy-Oxford,* 202**,** 94-99.